



Deposited via The University of York.

White Rose Research Online URL for this paper:

<https://eprints.whiterose.ac.uk/id/eprint/144999/>

Version: Accepted Version

Article:

Frost, William James, Samiepour, Marjan and Hirohata, Atsufumi (2019) Low-temperature crystallisation of Heusler alloy films with perpendicular magnetic anisotropy. *Journal of Magnetism and Magnetic Materials*. pp. 100-104. ISSN: 0304-8853

<https://doi.org/10.1016/j.jmmm.2019.04.008>

Reuse

This article is distributed under the terms of the Creative Commons Attribution-NonCommercial-NoDerivs (CC BY-NC-ND) licence. This licence only allows you to download this work and share it with others as long as you credit the authors, but you can't change the article in any way or use it commercially. More information and the full terms of the licence here: <https://creativecommons.org/licenses/>

Takedown

If you consider content in White Rose Research Online to be in breach of UK law, please notify us by emailing eprints@whiterose.ac.uk including the URL of the record and the reason for the withdrawal request.

Low-Temperature Crystallisation of Heusler Alloy Films with Perpendicular Magnetic Anisotropy

William Frost^{a,*}, Marjan Samiepour^a, Atsufumi Hirohata^a

^a*Department of Electronic Engineering, University of York, Heslington, YO10 5DD, UK*

Abstract

We demonstrate that perpendicular anisotropy can be induced in $\text{Co}_2\text{FeAl}_{0.5}\text{Si}_{0.5}$ by depositing the Heusler alloy on a tungsten seed layer. This is increased by elevating the deposition temperature to a moderate value up to 335 K. These perpendicular layers can be implemented into GMR devices, showing layer-thickness dependent switching without the use of an antiferromagnetic pinning-layer. These layers can be implemented into the manufacturing process of read-heads, where temperatures are limited.

Keywords

- Heusler Alloys
- Perpendicular Anisotropy
- Spintronics
- Spin-valves
- GMR

1. Introduction

Spintronic devices represent the most promising avenue for improved densities and functionality in information storage and hardware [1–3]. Heusler alloy based spintronic devices are a popular avenue for research to further recording densities above 2 TB/in² magnetic recording; for magnetic random-access memory (MRAM) [2] and for spin-torque oscillators [4] due to desirable properties such as high saturation magnetisations ($M_S > 1200$ emu/cm³), high Curie temperatures ($T_C > 800$ K) and predicted 100% spin polarisations [4–10]. However optimised growth of the Heusler alloys often requires a very specific and prohibitive set of conditions. For the most effective Heusler alloy giant magnetoresistance (GMR) and tunnelling magnetoresistance (TMR) devices, deposition slowly and epitaxially by methods such as molecular beam epitaxy (MBE) is used. Additionally the substrates used are often expensive MgO or sapphire single crystals [11]. Finally the structures are annealed at high temperatures up to 800 K for times measured in hours [5, 12]. However, significant progress has been made using ultra-high vacuum (UHV) sputtering processes, but the limitations of annealing still often apply.

This combination of prerequisites for an effective device prevent Heusler alloys from being technologically competitive at this time. This is especially prevalent in structures where perpendicular anisotropy is induced, whereby the tunnelling MgO barrier must be crystallised.

A lower temperature for the annealing or deposition of Heusler alloys with perpendicular anisotropy would be more efficient and protect other elements in device structures. Commercial devices often have an upper limit of 600 K with regards to annealing temperature [13]. Additionally lower temperatures prevent the diffusion and intermixing in multilayer devices. Previous work has shown that W seed layers induce a strong perpendicular anisotropy in Heusler alloy layers, massively increased by heating the substrate before deposition [14]. In this work systematic preheating of Si/SiO₂ substrates at temperatures between 292 K to 350 K has been utilised to crystallise $\text{Co}_2\text{FeAl}_{0.5}\text{Si}_{0.5}$ while maintaining perpendicular anisotropy, where the heat is applied for <10 min. This is extremely short compared to the typical annealing times required in general growth of Heusler alloys.

2. Experimental Procedures

All samples were deposited on Si (001) substrates using a PlasmaQuest High Target Utilisation Sputtering system (HiTUS) with a bias voltage of –900 V and a process pressure of 1.86 mTorr in order to maximise grain volume [15]. Prior to deposition the native SiO₂ layer was removed by exposure to the plasma. Initial samples had the substrate exposed to a heat source for a time of 0 s to 120 s before sputtering to preheat the samples, corresponding to substrate temperatures T_S of 292 K to 335 K. Pre-deposition heat treatment varies from post annealing in that it is a two-dimensional (2-D) growth process. In traditional annealing the grains must crystallise in three dimensions simultaneously which necessitates high temperatures and

*Corresponding author

Email address: william.frost@york.ac.uk (William Frost)

exposure time to provide the energy required for crystallisation. Contrastingly preheating only increases the surface energy of the grains upon deposition. This allows for a greater surface movement which in turn allows for greater crystallisation which takes place layer by layer during the sputtering process. As such this can be described as a 2-D process requiring lower temperatures and times than post-annealing.

GMR-style multilayers were deposited with the structure Si(001)//W (10 nm)/Co₂FeAl_{0.5}Si_{0.5} (12.5 nm)/W (1.2 nm)/Co₂FeAl_{0.5}Si_{0.5}(2.5 nm)/Ru (3 nm) where the two Heusler alloy layers are a "pinned" and "free" layer due to coercivity differences. The W layer was then replaced with silver for better layer separation and for the good band matching with Heusler alloys. The samples were magnetically characterised using ADE Model 10 and Lakeshore 7300 vibrating sample magnetometers (VSM) with a sensitivity of 1×10^{-6} emu and a field precision of 1 Oe. The sample mounts are rotational allowing for measurement both in-plane and out-of-plane. For crystallographic analysis a Rigaku SmartLab X-ray diffractometer (XRD) was used with a rotating 9 kW Cu-K_α source. A 6-axis goniometer was used to measure samples in both in-plane and out-of-plane geometries.

3. Results and Discussion

Figure 1a shows the θ - 2θ scans for the samples structures described in section 2 with increasing T_S . The (220) peak of Co₂FeAl_{0.5}Si_{0.5} at $\sim 45^\circ$ is seen to gradually increase in intensity as the crystallisation increases with temperature, with the relative intensity doubling from the lowest to highest deposition temperature. The 2θ position is close to that of the bulk, as indicated in the figure, and does not shift with increased crystallisation. The tungsten peak at $\sim 40^\circ$ shows dramatic increase in the relative intensity with a five-fold increase with increasing temperature. This indicates a dramatic increase in crystallisation which is also coupled with a phase transition from β -W to α -W followed by a relaxation towards the bulk location. The lattice constants and associated strains that were induced are shown in fig. 1b where the strain increases in the β -W phase, goes through a mixed phase at $T_S = 303K$ and transition into a strained α -W, with a strain value of of 0.8%.

The shift in the 2θ position of the W {110} reflection is not seen in equivalent in-plane $2\theta_\chi$ measurements. The W layer at low temperatures is being deposited with a distortion tetragonally out-of-plane, before relaxing with the application of heat. The increased deposition energy provided by a higher T_S allows for the tungsten lattice to relax to a bulk-like state. The size dependence of the crystallites can be determined using the Scherrer analysis of the two layers [16]. In the tungsten layer there is almost a twofold in the crystallite size from (5.4 ± 0.2) nm to (9.2 ± 0.1) nm with increasing T_S , following the trend of the crystallinity. Increased substrate temperature, and

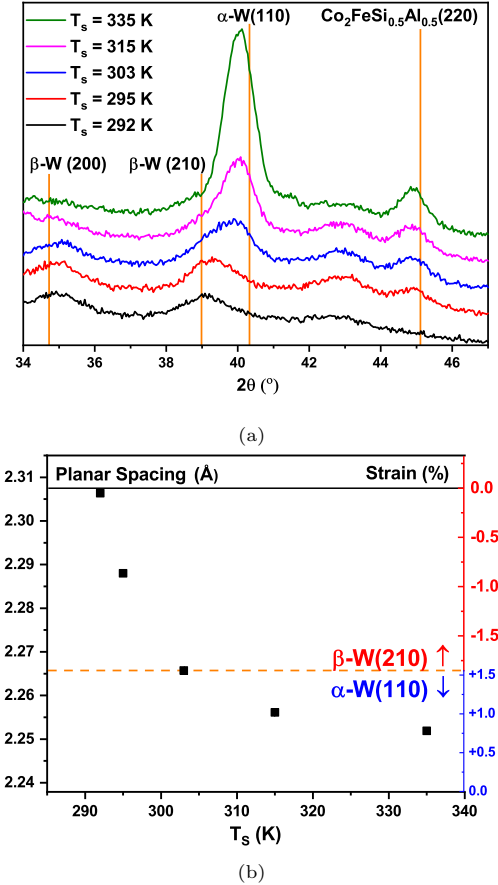


Figure 1: (a) θ - 2θ scans for samples with increasing preheating temperature and (b) the calculated lattice parameters and strain in the W lattice, with a phase transition from β -W to α -W.

therefore deposition energy, increases the mobility of incident ablated material. This in turn leads to an increased grain size as the mobile atoms cluster, resulting in fewer individual nucleation events for grain growth. As such the grain size in the material increases with T_S . Similarly in the Co₂FeAl_{0.5}Si_{0.5} layer there is a change from nanocrystalline or amorphous layer to a crystalline material with a crystallite size of (7.9 ± 0.1) nm as T_S increases. This change in crystallisation in the Heusler alloy layer has a significant effect on the magnetic properties of the samples.

Figure 2a shows the out-of-plane M - H loops for the samples. Firstly it is important to note that no antiferromagnetic coupling is achieved between the two layers regardless of T_S . Furthermore there is no evidence of layer dependent switching as would be expected from the two layer thicknesses [14]. There is a change in the magnetisation reversal process with increasing T_S , however. For the samples deposited above 300 K there is a large increase in H_C due to significant pinning strength up to to 1 kOe. This inhibits the domain rotation and domain wall motion until a nucleation field is reached, increasing with T_S . This increase is due to the increase in the grain size with the increasing deposition temperature. Furthermore the in-

crease in the nucleation field H_n could be due to changes in the interfacial properties.

The nucleation events in a granular thin film with small, single domain particles will occur at the edges of the film. The increase in the coercivity and H_n is therefore directly controlled by the anisotropy energy E_K

$$E_K = KV \quad (1)$$

where K is the anisotropy constant and V is the volume of the grain. Therefore as T_S increases the grain size, H_n will increase in order to overcome the anisotropy energy in the system. However in a granular material the grain volume is not indicative of the magnetic volume due to intergranular exchange coupling. This intergranular exchange coupling prevents the determination of K using the coherent rotation model on a hard-axis loop, as there is a non-zero coercivity both in- and out-of-plane as shown in fig. 2b. The shape of the in-plane hysteresis loop mimics that of the out-of-plane but with a reduced coercivity. The anisotropy in the films is therefore mixed and K must therefore be determined by methods such as ferromagnetic resonance (FMR).

Figure 2c shows an effective direct current demagnetisation (DCD) curve for the sample deposited at $T_S = 335$ K. A DCD curve is a measurement whereby the irreversible susceptibility of a sample can be determined, that is, the amount of magnetisation reversal which is not undone by removal of an applied field. Starting from a saturated state, increasingly large negative fields are applied and removed. The value of the remanence after each field is related to the irreversible component of the magnetisation [17]. The magnetisation of a body in a negative applied field is also time dependent, as thermal activation seeks to reverse all the magnetisation towards the equilibrium state at saturation [18]. This follows a logarithmic law where a field dependent coefficient describes the rate of magnetisation reversal at any given negative field. When combined with a DCD curve an activation volume can be determined for a film, as described below.

Due to the unquantifiable demagnetising field, H_d , the DCD curve can only be regarded as an effective one, not intrinsic as the remanence will be measured at a non-zero field [19]. However by taking the value for the irreversible susceptibility, χ_{irrev} , and a time-dependence coefficient, $S(H)$, at the remanent coercivity H_d can be ignored as the stray field from the sample is zero and a value for the activation volume V_a can be determined using

$$V_a = \frac{kT}{H_f M_S} \quad (2)$$

where kT is the thermal energy and H_f is the fluctuation field [20–22]. H_f is determined from the DCD and time dependence analysis using

$$H_f = \frac{S(H)}{\chi_{irrev}(H)} \quad (3)$$

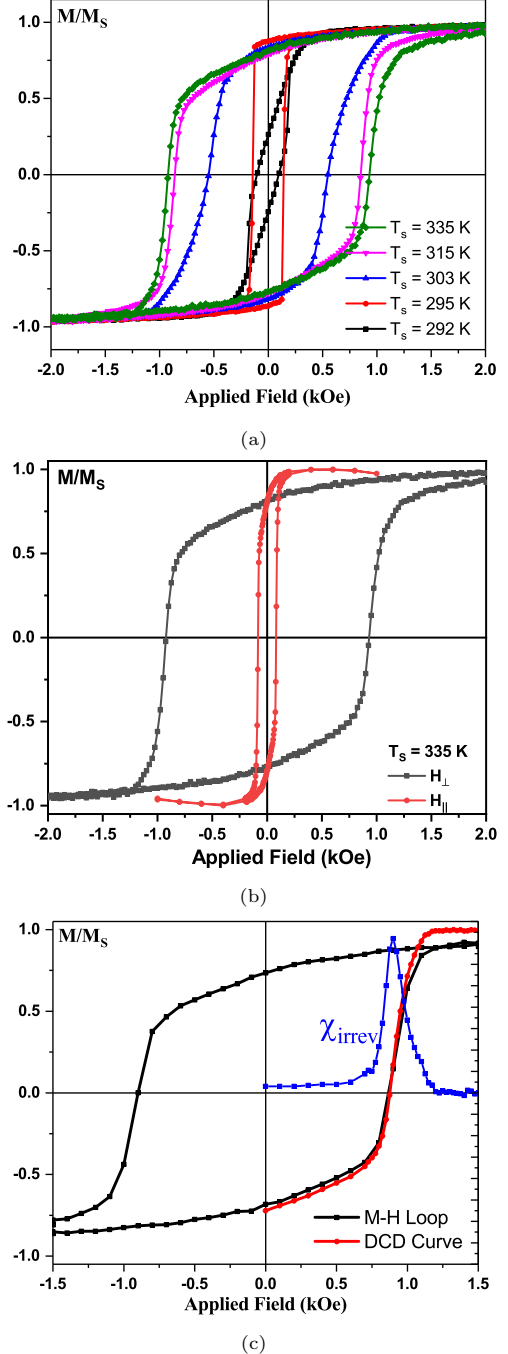


Figure 2: (a) Out-of-plane M - H loops for W/Co₂FeAl_{0.5}Si_{0.5} multilayers deposited with increasing substrate temperature T_S ; (b) the comparison of in- and out-of-plane MH -curves and (c) the DCD curve for the film deposited at 335 K.

From fig. 2c the diameter of the activation volume, D_a , is found to be (31 ± 2) nm. This is four times the crystallite diameter of 7.9 nm and is therefore direct evidence for the presence of strong intergranular exchange coupling in the film. Because of this strong intergranular exchange it is not surprising that a large portion of the magnetisation reversal occurs via nucleation.

In fig. 2c the DCD curve also closely follows the path of the M - H loop and as such the susceptibility of the film is almost entirely irreversible. This shows that there is a strong set of pinning sites in the film contributing to the coercivity and to the curvature of the M - H loop. This also increases the effective anisotropy for eq. (1), increasing H_n for the sample due to a higher energy barrier to reversal.

Silver has one of the best energy level matches to magnetic Heusler alloys for optimised GMR performance [11, 23]. Therefore to maximise any potential GMR the tungsten spacer layer has been replaced with one of silver, with thicknesses 3 nm and 5 nm. The samples were deposited at $T_S = 335$ K in order to maximise the coercivity difference between the two layers. Figure 3a shows the out-of-plane M - H loops for the two samples with silver spacer-layers. Both samples maintain perpendicular anisotropy despite the lack of a tungsten interface while showing a layer-thickness dependent switch, but with significantly different reversals.

The reversal in the sample with the 3 nm non-magnetic spacer-layer is more appropriate for device application for two reasons. Firstly the loop squareness, S , is 50% greater in this sample than the 5 nm spacer-layer, with values of $S_{3nm} = 0.75$ and $S_{5nm} = 0.5$ respectively. Secondly there is a significant domain rotational component of magnetisation reversal in the sample with a 5 nm spacer, which is indistinguishable between the two layers. This rotation means that no true antiparallel (AP) state is ever reached, further shown by the fact that the nucleation reversal takes place when the net magnetisation is negative. Therefore any GMR demonstrated in a device would be low and a 3 nm spacer-layer is more appropriate. However once more no AP coupling was achieved, the two coercivities are simply due to different anisotropies and pinning strengths in the two layers. In the film with a 5 nm spacer layer it is also possible that the perpendicular anisotropy has been reduced by the thicker spacer layer, resulting in two very distinct switching behaviours.

This set of optimised structure and deposition conditions was then used to fabricate nanopillar devices. The pillars were elliptical with sizes ranging from $1 \mu\text{m}$ by $0.5 \mu\text{m}$ to 150 nm by 100 nm . The MR -curve for the $1 \mu\text{m}$ by $0.5 \mu\text{m}$ pillar is shown in fig. 3b, with the field applied out-of-plane to the sample and measured at room temperature (RT). The magnetisation rotation and reversal to the AP state shown by the increase in resistivity to a maximum at 500 Oe agree with the magnetisation curves in fig. 3a, where the AP alignment is present. However, while the AP state is broad in the MH -loop, 500 Oe to 1000 Oe, the MR -curve has a sharp transition and the AP state is not

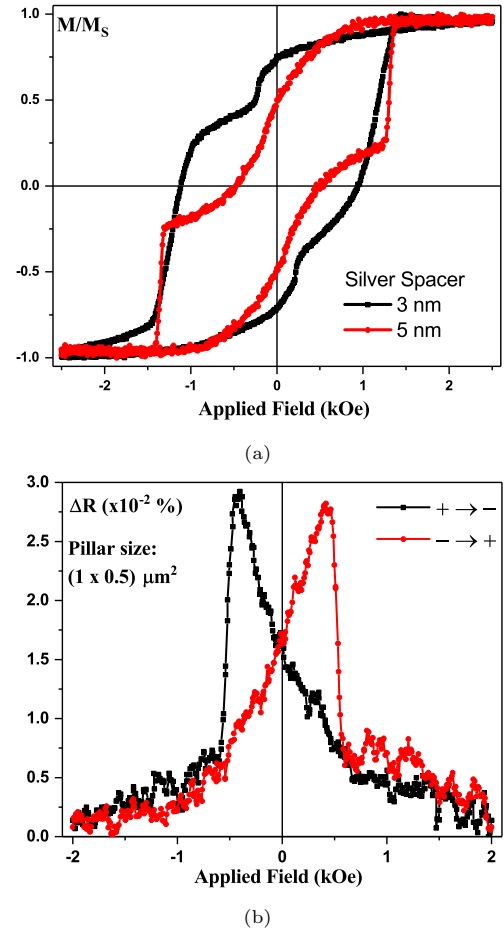


Figure 3: (a) Out-of-plane M - H loops for $W/\text{Co}_2\text{FeAl}_{0.5}\text{Si}_{0.5}/\text{Ag}$ multilayers deposited at $T_S=335$ K and (b) the corresponding MR -curve for a pillar with dimensions $(1000 \times 500) \text{ nm}^2$.

maintained at all. This is due to a decrease in H_n in the devices compared to the film. Edge damage to the pillars creates many imperfections, increasing the demagnetising field at device edges, reducing the switching field.

The observed GMR, however, is small with a value of only 0.03%. This is partially due to the rotation seen in fig. 3a; while there is a layer thickness dependent switch, due to magnetisation rotation in the layers there is never a true AP state. Furthermore the saturation magnetisation of the layers is significantly lower than the bulk M_S , 600 emu/cm³ compared to 1200 emu/cm³. This lower value may decrease the magnitude of the GMR. Additionally distributions of the crystallisation of the Heusler alloy, especially at interfaces, will reduce the spin polarisation from the bulk value, further reducing GMR. From M_S , we attribute the reduction of around 50% when compared to the bulk, which can be improved by further optimisation. It is therefore likely that only partial crystallisation of the Heusler alloy is achieved. Furthermore sample damage due to milling and patterning may further reduce M_S at device edges, further decreasing the GMR ratio.

4. Conclusions

We have shown that perpendicular anisotropy in the Heusler alloy Co₂FeAl_{0.5}Si_{0.5} can be induced using low-temperature deposition and a tungsten seed layer. Increasing the substrate temperature up to 335 K improves the crystallisation of the seed and magnetic layers as well as the anisotropy. However the crystallisation is still incomplete, with values of M_S and spin-polarisation below that of the bulk. These layers can be implemented into GMR devices by using a 3 nm silver spacer layer and a GMR ratio of 0.03% is observed at RT. Layer-thickness dependent switching is observed and spin-valve behaviour is obtained without the use of a pinning, antiferromagnetic layer.

5. Acknowledgements

This work was supported by Seagate Technology, Derry, Northern Ireland and the EPSRC-JPS Core-to-Core Programme (EP/M02458X/1) and JST CREST Programme (No. JPMJCR17J5). The authors would like to thank K. O'Grady (University of York), Marcus Ormston (Seagate) and Gabriel McCafferty (Seagate) for fruitful discussion.

References

[1] V. K. Joshi, *Spintronics: A contemporary review of emerging electronics devices*, Eng. Sci. Technol. an Int. J. 19 (3) (2016) 1503–1513. doi:10.1016/j.jestch.2016.05.002. URL <http://dx.doi.org/10.1016/j.jestch.2016.05.002>

[2] A. Hirohata, H. Sukegawa, H. Yanagihara, I. Zutic, T. Seki, S. Mizukami, R. Swaminathan, *Roadmap for Emerging Materials for Spintronic Device Applications*, IEEE Trans. Magn. 51 (10) (2015) 1–11. doi:10.1109/TMAG.2015.2457393. URL <http://ieeexplore.ieee.org/document/7160747/>

[3] A. Hirohata, K. Takanashi, *Future perspectives for spintronic devices*, J. Phys. D. Appl. Phys. 47 (19) (2014) 193001. doi:10.1088/0022-3727/47/19/193001. URL <http://iopscience.iop.org/article/10.1088/0022-3727/47/19/193001/pdf>

[4] T. Seki, Y. Sakuraba, H. Arai, M. Ueda, R. Okura, H. Imaura, K. Takanashi, *High power all-metal spin torque oscillator using full Heusler Co₂(Fe,Mn)Si*, Appl. Phys. Lett. 105 (9). doi:10.1063/1.4895024. URL <http://dx.doi.org/10.1063/1.4895024http://aip.scitation.org/toc/apl/105/9>

[5] T. M. Nakatani, N. Hase, H. S. Goripati, Y. K. Takahashi, T. Furubayashi, K. Hono, *Co-Based Heusler Alloys for CPP-GMR Spin-Valves With Large Magnetoresistive Outputs*, IEEE Trans. Magn. Trans. Magn. 48 (5) (2012) 1751–1757. doi:10.1109/tmag.2011.2174436.

[6] Z. Diao, M. Chapline, Y. Zheng, C. Kaiser, A. Ghosh Roy, C. J. Chien, C. Shang, Y. Ding, C. Yang, D. Mauri, Q. Leng, M. Pakala, M. Oogane, Y. Ando, *Half-metal CPP GMR sensor for magnetic recording*, J. Magn. Mater. 356 (2014) 73–81. doi:10.1016/j.jmmm.2013.12.050. URL <http://dx.doi.org/10.1016/j.jmmm.2013.12.050>

[7] K. Nikolaev, P. Kolbo, T. Pokhil, X. Peng, Y. Chen, T. Ambrose, O. Mryasov, *"All-Heusler alloy" current-perpendicular-to-plane giant magnetoresistance*, Appl. Phys. Lett. 94 (22) (2009) 222501. doi:10.1063/1.3126962. URL <http://aip.scitation.org/doi/10.1063/1.3126962>

[8] Y. Sakuraba, S. Kokado, Y. Hirayama, T. Furubayashi, H. Sukegawa, S. Li, Y. K. Takahashi, K. Hono, *Quantitative analysis of anisotropic magnetoresistance in Co₂MnZ and Co₂FeZ epitaxial thin films: A facile way to investigate spin-polarization in half-metallic Heusler compounds*, Appl. Phys. Lett. 1041 (10) (2014) 172407–7. doi:10.1063/1.4874851. URL <http://dx.doi.org/10.1063/1.4874851>

[9] T. Graf, C. Felser, S. S. P. Parkin, *Simple rules for the understanding of Heusler compounds*, Prog. Solid State Chem. 39 (1) (2011) 1–50. doi:10.1016/j.progsolidstchem.2011.02.001. URL <http://dx.doi.org/10.1016/j.progsolidstchem.2011.02.001>

[10] Y. K. Takahashi, N. Hase, M. Kodzuka, A. Itoh, T. Koganezawa, T. Furubayashi, S. Li, B. S. D. C. S. Varaprasad, T. Ohkubo, K. Hono, *Structure and magnetoresistance of current-perpendicular-to-plane pseudo spin valves using Co₂Mn(Ga_{0.25}Ge_{0.75}) Heusler alloy*, J. Appl. Phys. 113 (22) (2013) 0–7. doi:10.1063/1.4809643.

[11] T. Furubayashi, K. Kodama, H. Sukegawa, Y. K. Takahashi, K. Inomata, K. Hono, *Current-perpendicular-to-plane giant magnetoresistance in spin-valve structures using epitaxial Co₂FeAl_{0.5}Si_{0.5}/Ag/Co₂FeAl_{0.5}Si_{0.5} trilayers*, Appl. Phys. Lett. 93 (12) (2008) 122507. doi:10.1063/1.2990647. URL <http://aip.scitation.org/toc/apl/93/12>

[12] J. Sato, M. Oogane, H. Naganuma, Y. Ando, *Large Magnetoresistance Effect in Epitaxial Co₂Fe_{0.4}Mn_{0.6}Si/Ag/Co₂Fe_{0.4}Mn_{0.6}Si Devices*, Appl. Phys. Express 4 (11) (2011) 113005. doi:10.1143/APEX.4.113005.

[13] K. Suzuki, B. W. Smith, *Microlithography: science and technology*, CRC Press, 2007.

[14] W. Frost, A. Hirohata, *Heusler alloys with bcc tungsten seed layers for GMR junctions*, J. Magn. Mater. 453 (2018) 182–185. doi:10.1016/j.jmmm.2018.01.015.

[15] M. Vopsaroiu, M. J. Thwaites, S. Rand, P. J. Grundy, K. O'Grady, *Novel sputtering technology for grain-size control*, IEEE Trans. Magn. 40 (4 II) (2004) 2443–2445. doi:10.1109/TMAG.2004.828971. URL <http://ieeexplore.ieee.org/document/1325532/>

[16] A. L. Patterson, *The scherrer formula for X-ray particle size determination*, Phys. Rev. 56 (10) (1939) 978–982. arXiv:arXiv:1011.1669v3, doi:10.1103/PhysRev.56.978. URL <https://journals.aps.org/pr/pdf/10.1103/PhysRev.56.978>

- [17] K. O'Grady, V. G. Lewis, D. P. E. Dickson, R. Goldfarb, **Alternating gradient force magnetometry: Applications and extension to low temperatures (invited)**, *J. Appl. Phys.* 731 (10) (1993) 15110–1241. doi:10.1063/1.1141451.
URL <http://dx.doi.org/10.1063/1.353613>
- [18] R. Street, J. C. Woolley, P. B. Smith, **Magnetic Viscosity under Discontinuously and Continuously Variable Field Conditions**, *Proc. Phys. Soc. Sect. B* 65 (9) (1952) 679–696. doi:10.1088/0370-1301/65/9/305.
URL <http://iopscience.iop.org/article/10.1088/0370-1301/65/9/305/pdf>
- [19] J. G. T. te Lintelo, J. C. Lodder, **Influence of demagnetization in remanence curves of magnetic thin films**, *J. Appl. Phys.* 77 (12) (1995) 6416–6425.
URL <https://ris.utwente.nl/ws/portalfiles/portal/6982904/LINTEL01995.PDF>
- [20] R. Street, J. C. Woolley, **A Study of Magnetic Viscosity**, *Proc. Phys. Soc. Sect. A* 62 (9) (1949) 562–572. doi:10.1088/0370-1298/62/9/303.
URL <http://iopscience.iop.org/article/10.1088/0370-1298/62/9/303/pdf>
- [21] L. Néel, **Le traînage magnétique**, *J. phys. radium* 12 (1951) 339–351. doi:10.1051/jphysrad:01951001203033900.
URL <http://www.edpsciences.org/10.1051/jphysrad:01951001203033900>
- [22] E. Wohlfarth, **The coefficient of magnetic viscosity**, *J. Phys. F Met. Phys.* 14 (14) (1984) L155–L159. doi:10.1088/0305-4608/14/8/005.
URL <http://iopscience.iop.org/article/10.1088/0305-4608/14/8/005/pdf><http://iopscience.iop.org/0305-4608/14/8/005>
- [23] Y. Sakuraba, M. Ueda, S. Bosu, K. Saito, K. Takanashi, **CPP-GMR study of half-metallic full-Heusler compound Co₂(Fe, Mn)Si**, *J. Magn. Soc. Japan* 38 (2014) 45–49.
URL https://www.jstage.jst.go.jp/article/msjmag/38/2-2/38_{_}1403R001/{_}.pdf